# Putting a spin on it: amyloid aggregation from oligomers to fibrils

Zurlo, E.

# 3 Tracking amyloid oligomerization with monomer resolution using a 13-amino acid peptide with a backbone-fixed spin label

Amyloid oligomers are suspected as toxic agents in neurodegenerative disease, they are transient and often heterogeneous, making them difficult to detect. Here we show an approach to track the development of amyloid oligomers in situ by room temperature, continuous wave (cw) 9 and 95 GHz EPR. Three amyloid peptides with the 2,2,6,6-tetramethyl-N-oxyl-4-amino-4-carboxylic acid (TOAC) spin label were synthesized by solid phase peptide synthesis: T0EZ (TKVKVLGDVIEVGG) with the TOAC (T) at the N-terminus, T5EZ, with TOAC in the middle (KVKVTGDVIEVG) and T12EZ , with TOAC at the C-terminus (KVKVLGDVIEVTG). These sequences are derived from the K11V (KVKVLGDVIEV) amyloid peptide, which self-aggregates to oligomers with a β-sheet configuration (Laganowsky, A. et al., Science 335, 1228–1231 (2012)). To monitor oligomerization, the rotational correlation time ($\tau_r$) is measured by cw-EPR. For the backbone-fixed TOAC label that is devoid of local mobility, $\tau_r$ should reflect the rotation and thereby the size of the peptide, resp. oligomer. For T5EZ a good match between the $\tau_r$ measured and the size of the peptide is obtained, showing the validity of the approach. One of the three peptides (T0EZ) aggregates (circular dichroism), whereas the other two do not. Since also the respective MTSL (S-(1-oxyl-2,2,5,5-tetramethyl-2,5-dihydro-1H-pyrrol-3-yl)methyl methanesulfonothioate) labelled peptides fail to aggregate, molecular crowding due to the label, rather than the helix-inducing properties of TOAC seem to be responsible. Following in situ oligomer formation of T0EZ by the change in rotational correlation time, two oligomers are observed, a 5-6 mer and a 15-18 mer. The EPR approach, particularly 95 GHz EPR, enables to follow oligomerization one monomer at a time, suggesting that the cw-EPR approach presented is a novel tool to follow amyloid oligomerization with high resolution.

Zurlo, E., Gorroño Bikandi, I., Meeuwenoord, N. J., Filippov, D. V. & Huber, M. Tracking amyloid oligomerization with monomer resolution using a 13-amino acid peptide with a backbone-fixed spin label. *Phys. Chem. Chem. Phys.* **21**, 25187–25195 (2019).

# 3.1 Introduction

Amyloid aggregation is a central factor in amyloidogenic neurodegenerative diseases. Such diseases are widespread and so far most of them cannot be cured. One obstacle is the gap in knowledge about the physical chemistry of amyloid aggregation. Amyloid aggregation is the process in which the amyloid peptide self-assembles. The thermodynamic end-point of the aggregation is the β-sheet fibril, the main component of the plaques in the brains of patients, so far the main diagnostic feature for neurodegenerative disease.[96,97] Meanwhile, evidence is growing that amyloid oligomers, not fibrils, are the more toxic species[14–19]. Oligomers are aggregates of up to tens to hundred monomers. They can be on-pathway to fibrils, i.e. nuclei of fibrilization or off-pathway, meaning that they do not directly participate in fibril formation. Oligomers can differ in size, i.e. number of peptides, structure, stability and physico-chemical properties. Their transient nature and heterogeneity make the oligomers difficult to track.[16,96,98] Harmful oligomers are targets for drugs against neurodegenerative disease, generating a pressing need to design methods to determine the oligomers' mode of formation and structure. In particular, methods are needed to detect oligomers in situ, i.e. methods that show, which oligomers are formed, their relative concentration and how these parameters develop over time.

Here we explore the potential of liquid-solution, room temperature Electron Paramagnetic Resonance (EPR) at standard (9 GHz) and high (95 GHz) EPR frequencies to attain this goal.

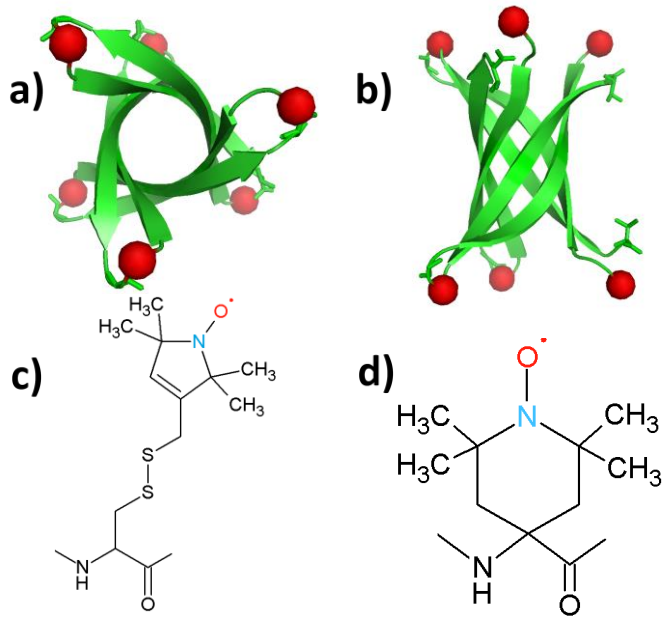


***Figure 3.1*** *Structure of K11V oligomer and relevant spin labels. a),b) Oligomer structure of K11V (PDB **3SGO**), showing the 2,2,6,6-tetramethyl-N-oxyl-4-amino-4-carboxylic acid (TOAC) location for T0EZ (red dots). For details, see text. View in b) is rotated 90º with respect to a). c) Molecular structure of the MTSL spin label attached to a cysteine side-chain. d) Molecular structure of the TOAC spin label.*

These techniques make it possible to follow oligomer formation by detecting the size of the oligomers: For continuous-wave EPR (cw EPR) in liquid solution, the spectral lineshape is a sensitive indicator for the rotational correlation time ($\tau_r$) of an object, and it covers the time range from 0.03 ns to several ns[47,99–101]. As will be described below, this $\tau_r$ range matches well with the $\tau_r$ expected for the sizes of typical amyloid-forming oligomer peptides and their aggregates at room temperature in aqueous solution. Therefore, we expect to be able to track oligomer formation via the increase in $\tau_r$.

To perform EPR on amyloid peptides, the peptides need to be spin labeled. Conventionally, spin labels, like the S-(1-oxyl-2,2,5,5-tetramethyl-2,5-dihydro-1H-pyrrol-3-yl)methyl methanesulfonothioate (MTSL) label, are introduced via spin-label site-directed mutagenesis, which results in structures like Figure 3.1c[47,59,100,101]. While this approach is universal, the local mobility is a disadvantage in the study of amyloid aggregation: Rotation about the single bonds linking the nitroxide to the protein backbone dominates the motion and makes the measurement insensitive to peptide/oligomer size. We therefore use the backbone-fixed TOAC spin label (Figure 3.1d), which is incorporated into the peptide during solid phase peptide synthesis (SPPS)[62,75–78,102–106]. In these constructs, the nitroxide, containing the unpaired electron, is directly linked to the protein backbone, and therefore its $\tau_r$ will follow the peptide rotation much more closely than the nitroxide in MTSL.

As model system we use the K11V peptide (Figure 3.1a,b), a short peptide, the sequence of which is derived from the αB crystallin protein.[67] Such peptides, comprising 5-15 aminoacids have proven extremely useful for mechanistic studies. They show the essential properties of the protein they are derived from, but their smaller size is helpful to model their aggregation by MD methods, and, pioneered by the Eisenberg group, enable investigation by X-ray crystallography. The K11V peptide was shown to form toxic amyloid oligomers that could be crystallized. The X-ray structure shows a hexamer in β-sheet conformation, a β-barrel (Figure 1a,b).[67] Apparently, K11V forms fibrils much more slowly than other amyloid peptides, making it ideal to study oligomerization.

***Table 3.1*** *Sequences of peptides. The spin label TOAC (2,2,6,6-tetramethyl-N-oxyl-4-amino-4carboxylic acid) is abbreviated as T.*

| | **sequence** |
|---|---|
| **K11V** | K V K V L G D V I E V |
| **T0EZ** | **T** K V K V L G D V I E V G |
| **T5EZ** | K V K V **T** G D V I E V G |
| **T12EZ** | K V K V L G D V I E V **T** G |
| **EZ** | K V K V L G D V I E V G G |

We synthesized four variants of the K11V peptide, a wild type analog (EZ) and three variants with the TOAC spin label in different positions (Table 3.1). We show that in spite

of the α-helix inducing property of TOAC[75–79,82,93] one of the three TOAC constructs aggregates to oligomers. We demonstrate that our approach enables to follow aggregation in time with, in principle, monomer-size resolution.

# 3.2 Materials and methods

## *3.2.1 Synthesis and characterization of peptides*

All chemicals were commercial products of the best quality available and, unless otherwise indicated, they were used without any further purification. The EZ peptide was purchased from tebu-bio (Heerhugowaard, The Netherlands).

9-Fluorenylmethoxycarbonyl(Fmoc)-amino acids, Fmoc-Gly-Wang Tentagel resin and the other chemicals used for the solid phase peptide synthesis were purchased from Sigma Aldrich. 2,2,6,6-Tetramethylpiperidine-N-oxyl-4-(9-fluorenylmethyloxycarbonyl-amino)-4-carboxylic acid (Fmoc-TOAC-OH) and H-Gly-Wang resin were supplied by Iris Biotech (Marktredwitz, Germany).

The peptide sequences were assembled on AB433A Peptide Synthesizer (Applied Biosystems, Foster City, CA, USA), using 0.05 mmol of Gly-Wang resin (substitution 0.5 mmol/g). For all amino acids except TOAC we use 5 equivalents (0.25 mmol) of each AA for the synthesis. Deprotection by Fmoc was done 4 times (3 minutes each) by adding 2.5 mL of a solution of 20 % piperidine (PIP) in N-methylpyrrolidone (NMP). Couplings were performed using *2-(6-Chloro-1H-benzotriazole-1-yl)-1,1,3,3-tetramethylaminium hexafluorophosphate* (HCTU) as an activator and N,N-Diisopropylethylammine (DIPEA) as base. We used 1 equivalent of HCTU and 2 equivalents of DIPEA for 1 equivalent of AA. 1 mL of a solution of HCTU (0.25 M in NMP), 0.5 mL of a solution of DIPEA (1 M in NMP) and 0.5 mL of NMP were added to the resin for the coupling reactions. Each coupling reaction lasted 2 hrs.

The TOAC spin label was treated differently. Only 2 equivalents of AA were added for 1 equivalent of resin. Instead of HCTU, 1-[Bis(dimethylamino)methylene]-1H-1,2,3-triazolo[4,5-b]pyridinium 3-oxid hexafluorophosphate (HATU) was used as activator and 400 µL of its solution (0.5 M in NMP) were put directly inside the cartridge with the spin label together with 600 µL of NMP. The coupling in this case lasted 4 hrs. For the AA introduced immediately after the TOAC we used a double coupling, keeping the same conditions as for the rest of the sequence. The Fmoc absorption at 301 nm was followed to check the status of the synthesis after each coupling step.

At the end of the synthesis the resin was dried by washing it with dichloromethane (DCM). To cleave the peptide from the resin 2 mL of a solution 95% trifluoroacetic acid (TFA) + 5% water was used. A small amount of peptide was cleaved from the resin and

characterized by LC-MS. Unless otherwise indicated, the peptides were purified by semi-preparative HPLC.

Analytical HPLC separation was carried out on a LCQ Advantag Thermo Finnigan LC-MS system with UV-Vis and Ion-trap mass detectors. The column used was a C-18 Gemini (4.6 x 50 mm, 3 μm particle size) from Phenomenex (Torrance, California). The mobile phase A ($H_2O$), B (acetonitrile, MeCN) and C (aqueous 1 % TFA) was used for preparing ternary gradients. Elution condition: A 80 % B 10 % C 10-90 %, linear gradient B 18-33 % in 10 min. Flow rate 1 mL/min.

Crude peptide purifications were performed on a Gilson HPLC preparative system with a semipreparative Gemini $C_{18}$ column (10 x 250 mm) from Phenomenex with UV-Vis detector. The mobile phase A ($H_2O$) and B (acetonitrile, MeCN) and C (aqueous 1 % trifluoroacetic acid, TFA) were used for preparing binary gradients. Elution condition: A 82 % B 18 %, linear gradient B 18-33 % in 10 min, Flow rate 5 mL/min.

The lyophilization was done on a Christ Alpha 2-4 LO lyophilizer (Salm&Kipp, Breukelen, Netherlands) with a Christ RVC 2-25 rotor. All TOAC peptides had a high level of purity as shown by single band elution and mass spectrometry.

T5EZ: yield 2.0%; LC-MS (C18) $^{t}R$ 4.56 min; purity $>$ 95%; Mass: calculated for $C_{61}H_{108}N_{15}O_{18}$ $[M+H]^+$ 1339.61, found: 1339.47

T0EZ: yield 10.8%; LC-MS (C18) $^{t}R$ 4.68 min; purity $>$ 95%; Mass: calculated for $C_{69}H_{122}N_{17}O_{20}$ $[M+H]^+$ 1453.794 , found: 1453.53

T12EZ: yield 1.4%; LC-MS (C18) $^{t}R$ 4.85 min; purity $>$ 95%; Mass: calculated for $C_{69}H_{122}N_{17}O_{20}$ $[M+H]^+$ 1453.794 , found: 1453.60

## *3.2.2 Protocol for the aggregation experiments*

Samples were prepared as follows: The powder of the lyophilized spin-labelled EZ peptides was dissolved in Milli-Q water, in order to get a peptide concentration of 500 μM by weight. Aggregation experiments were carried out during one week. After an initial measurement taken at the time the spin-labelled-peptide powder was diluted in Milli-Q water ($t = 0$), samples with a total volume of 560 μL in 1.5 mL Eppendorf tubes were aggregated on a thermomixer (Eppendorf, Thermomixer comfort, Waltham, MA USA) with a speed of 1000 rpm at 293 K. At each time point a 20 μL sample was drawn for an EPR measurement, one of 40 μL for CD and 10 μL were frozen for future experiments, e.g. 95 GHz EPR and ThioT fluorescence. The time points were: one hour, four hours, one day (24 h), two days (48 h), three days (72 h) and seven days (168 h).

### *3.2.3 ThioflavinT fluorescence*

The samples were monitored by the standard Thioflavin T (ThioT) fluorescence assay[107]. In summary, 5 µL of sample solution were dissolved into 2 mL of a solution 5 µM of ThioT and mixed for 30 seconds. The sample was excited at 457 nm and the fluorescence was observed in the range of 475 nm to 600 nm (Varian Cary Eclipse, San Jose, CA, USA). The fluorescence increase was measured with respect to the ThioT blank without the peptide.

### *3.2.4 EPR measurement conditions*

The 9 GHz, continuous-wave EPR spectra were recorded using an ELEXSYS E680 spectrometer (Bruker, Rheinstetten, Germany). The measurements were done under the following conditions: room temperature, a microwave power of 0.63 mW and a modulation amplitude of 0.15 mT at a modulation frequency of 100 kHz. The time expended on each measurement was adapted according to the spectral lineshape, i.e., the aggregation time. For the starting point of the aggregation 30 min were expended, and up to 5 h for samples at the end of the aggregation series. Glass micropipettes of a volume of 50 µL (Blaubrand Intramark, Wertheim, Germany) were filled with 20 µL of the sample for each measurement. The spin concentration was determined by comparing the double integral of the EPR spectra with the double integral of a reference sample (MTSL, 100 µM). The spin concentrations were ≈ 100 µM for a total concentration of peptide of 500 µM.

The 95 GHz EPR spectra were recorded at room temperature on a Bruker ELEXSYS E680 spectrometer using a home-built probehead with a single-mode cavity specially designed for cw measurements. Acquisition parameters: microwave frequency 94.04 GHz, microwave power 0.63 µW, modulation amplitude 1 mT, modulation frequency 6 kHz. Total measurement time: approximately 5 hours.

### *3.2.5 Simulations of EPR spectra*

MATLAB (version 9.4.0.813654, R2018a, The MathWorks, Inc., Natick, MA, USA) and the EasySpin package (5.2.4) were used for simulations of the EPR spectra.[48] The parameters of the simulation were manually adjusted to agree best with the experimental spectra. For all simulations, an isotropic rotation of the nitroxide ($S = 1/2$) was utilized. The following g-tensor values were used: $g = [2.0086\ 2.0059\ 2.0020]$. These values were

obtained from the simulation of the 275 GHz EPR spectrum of a frozen solution (100 K) of the peptide, using the "Pepper" algorithm in EasySpin, and we used these values for all other simulations. The principal values of the $^{14}N$ hyperfine coupling tensor were $A_{xx} = A_{yy} = 13$ MHz and $A_{zz} = 110$ MHz.[108] The spectra were simulated with a superposition of three components: a fast fraction using the "Garlic" function, a medium and a slow fraction using the "Chili" function. For the 9 GHz spectra, a Gaussian component with a linewidth of 0.12 mT was used for the fast component, and 1 mT for the medium and slow components. For the 95 GHz spectra, a Gaussian line with a width of 0.5 mT was used for the fast component, whereas for the medium and slow components a mix of Gaussian and Lorentzian lineshape with a width of 0.1 mT was applied. The $\tau_r$ of the fast component was chosen by simulating the narrow lines of the $t = 0$ measurements and then kept constant for all other simulations. Optimal $\tau_r$ values of the medium and slow components were derived from later time-point spectra and then kept constant for the entire series. For each time point, the relative contribution of the three components was optimized considering both 9 and 95 GHz spectra, for more details see SI.

### *3.2.6 Interpretation of $\tau_r$ values and molecular volumes*

We used the Stokes-Einstein equation to interpret the $\tau_r$ values. This implies a spherical approximation for the particles:

$$\tau_r = \frac{4\pi\eta\alpha^3}{3kT} = \frac{\eta}{kT} V_{EPR} \tag{3.1}$$

In Eqn. (3.1) $k$ is the Boltzmann constant, T is the temperature (293 K), $\eta$ is the viscosity of the solvent (1.02 cP for water) and α is the hydrodynamic radius. The resulting volumes are referred to as $V_{EPR}$ in the text.

The experimentally determined values of the volume ($V_{EPR}$) have to be compared to the volumes of the peptide and its oligomers. There are two approaches to derive such estimates:

Method (i) uses the molecular weight (MW) and derives the volume assuming a certain density of the proteins using Eqn. (3.2), and we refer the volume obtained as $V_{MW}$. The second approach (ii) uses the dimension of the K11V oligomer (cylindrin) to derive the to-be-expected volume of the peptide. In the following we describe these two approaches.

Method (i):

$$V_{MW} = \frac{MW}{N_A \rho} \tag{3.2}$$

Here, ρ is the protein density, $N_A$ is Avogadro's constant and $V_{MW}$ is the way we will address the volume obtained by this approach. To determine the number of monomers in the oligomers, the apparent molecular weight corresponding to $V_{EPR}$ is calculated according to:

$$MW_{app,i} = V_{EPRi} N_A \rho \tag{3.3a}$$

$$n_i = \frac{MW_{appi}}{MW_{T0EZ}} \tag{3.3b}$$

and the number of monomers in species i, $n_i$, by dividing by the MW of the peptide T0EZ, $MW_{T0EZ}$.

The density of proteins of MW > 20 kDa is generally assumed to be $\rho = 1.35$ g/cm$^3$, [109] however also other values were reported for smaller proteins, such as 1.50 g/cm$^3$, [110]. In the SI, the influence of different ρ values is discussed and the resulting spread in $n_i$ is included in the error estimation. The molecular weight of a monomer of T0EZ and of T12EZ is 1452.60 g/mol and for T5EZ 1338.47 g/mol.

Method (ii) uses the dimension of the oligomer of the K11V peptide that had been determined by X-ray crystallography)[67].

$$V_{XR} = \frac{\pi r^2 h}{6} \tag{3.4}$$

The volume of the oligomer is approximated as a cylinder of radius r, 11 Å, and a height, h, of 22 Å. The volume obtained agrees well with the volume obtained by HYDRONMR, see SI. The volume of the monomer obtained by Eqn. (3.4) is called $V_{XR}$.

# 3.3 Results

To determine the aggregation of the different TOAC constructs, Circular Dichroism (CD) spectroscopy was performed for samples taken at different time points of the aggregation. Initially all constructs display random coil CD spectra and T0EZ shows increasing β-sheet character over time, whereas T5EZ and T12EZ remain unchanged. More details of CD spectra on T0EZ are given in the SI (see also SI chapter 2), including the analysis using BeStSel[111,112]. To test for the formation of fibrils, ThioT fluorescence[107] was measured. None of the samples showed ThioT activity. This is to be expected as ThioT fluorescence requires linear cross-beta sheet structures of minimally six peptides in a row[113], a requirement that the highly curved β-sheet in the β-barrel oligomer (Figure 3.1) does not fulfill. Therefore, the absence of ThioT fluorescence shows only that no fibrils are formed, however it does not exclude oligomers. For T0EZ these findings are consistent with a β-sheet oligomer: It displays β-sheet structure in CD and does not show

ThioT fluorescence, which excludes that β-sheet fibrils are formed. In the following, we first describe the EPR properties and the aggregation behavior of T0EZ and then the properties of the other two constructs, T5EZ and T12EZ.

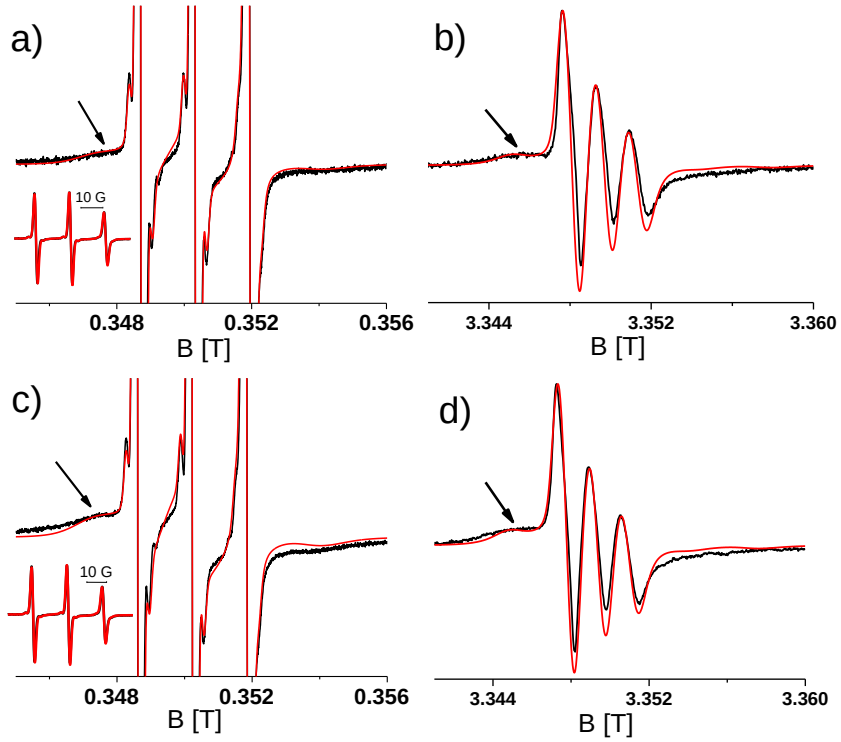


***Figure 3.2*** *Room temperature 9 and 95 GHz EPR spectra of T0EZ at different time points of aggregation. a) c) 9 GHz EPR spectra. Full spectra: Inset. Zoomed-in spectra: Amplitude expanded ten-fold with respect to inset. b) d) 95 GHz spectra. Spectra a) and b): Start of aggregation (t = 0). c) and d): At 48 hours of aggregation. Black: Experimental spectra. Red: Simulated spectra. Note that at 95 GHz the signal appears at around ten times higher field* $B_0$.

Figure 3.2 shows the EPR spectra of T0EZ at 9 and 95 GHz obtained at two time points of aggregation; at the start (Figure 3.2a and b) and after 48 hours of aggregation (Figure 3.2c and d), the spectra of all time points are collected in Figure S3.1. The 9 GHz EPR spectra are dominated by three narrow lines (see inset) of a nitroxide in fast rotation. The arrow marks an additional broad component, representing a component with lower mobility. In the 95 GHz EPR spectra (Figure 3.2b and 3.2d), taken at around ten times higher field, this component is better separated from the three-line pattern than at 9 GHz EPR. The spectra at the two time points differ mostly in the relative amplitude of the broad with respect to the narrow component. The broad component has a higher amplitude in Figure 3.2c and d than that in Figure 3.2a and b. To quantitate the changes in the EPR spectra, we performed spectral simulations.

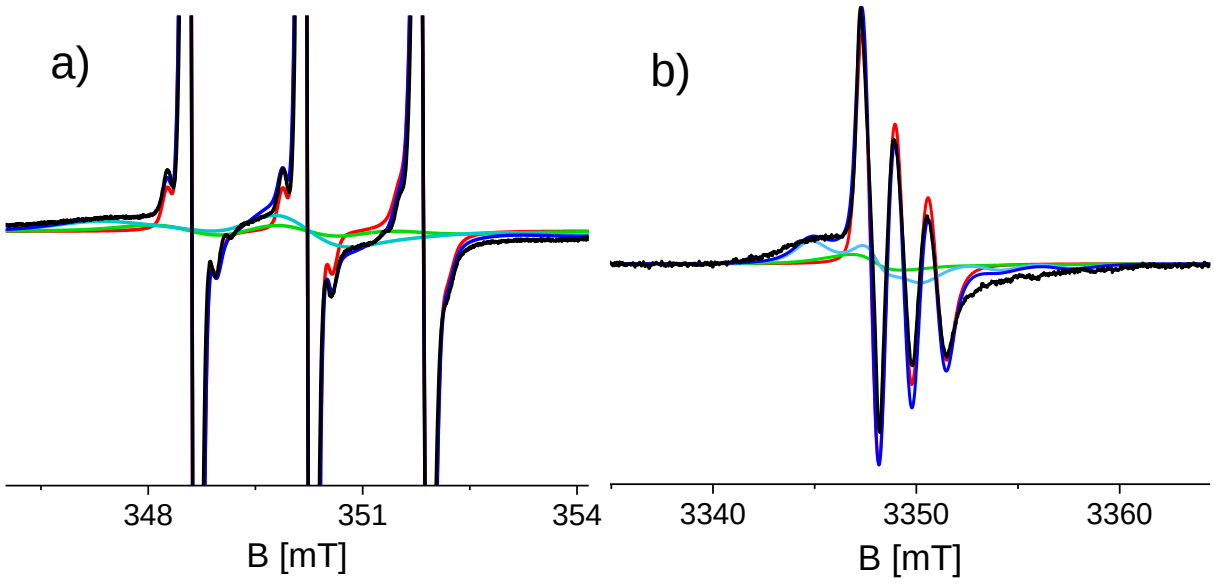


***Figure 3.3*** *Spectral components used in the simulation of the 9 and 95 GHz EPR spectra of T0EZ ( 48 hours of aggregation). Experimental spectra (black), fast component (red), medium component (green), slow component (light blue). Total simulation (dark blue). For details see text.*

Simulations required minimally three components with different rotational correlation times ($\tau_r$). Figure 3.3 shows the shape of these components for the spectra shown in Figure 3.2c and d, i.e. at 48 hours of aggregation. The contribution with the longest $\tau_r$ (light blue) gives rise to the broad features marked in Figure 3.2 by the arrows. The $\tau_r$ values are given in Table 3.2. To simulate the entire series of time points, the $\tau_r$ of each component was kept constant and only the relative amount of the components was varied throughout the time series. Furthermore, the 9 and 95 GHz EPR spectra for the same time point were simulated with the same relative amounts of the components. The higher resolution of 95 GHz EPR makes it easier to detect the slow components. Compare Figure 3.2b and d (95 GHz) with 3.2a and c (9 GHz). The slow and medium components are related to aggregates and the amount by which they contribute to the spectra in time increases as shown in Figure 3.4.

***Table 3.2 .*** *Rotational correlation times of T0EZ from the simulation of the EPR spectra, and corresponding molecular volumes ($V_{EPR}$). Using monomer volumes from different sources (see text), the number of the peptides in the oligomer is derived.*

| **Components** | **$\tau_r$ [ns]** | **$V_{EPR}$ [nm$^3$][a]** | **Number of monomers in aggregate** | |
|---|---|---|---|---|
| | | | From MW[b] | From XR[c] |
| **Fast** | 0.16 ± 0.004 | 0.65 ± 0.02 | - | - |
| **Medium** | 2.00 ± 0.20 | 8.08 ± 0.81 | 5 ± 1 | 6 ± 1 |
| **Slow** | 6.31 ± 0.70 | 25.49 ± 2.83 | 15 ± 2 | 18 ± 2 |

a) From Stokes-Einstein (Eqn. 1).
b) From protein density (Eqn. 2) using ρ = 1.35 g/cm$^3$, for further uncertainties in these numbers, see text.
c) From X-ray crystallography (Eqn. 3) , for further uncertainties in these numbers, see text.

Using the Stokes-Einstein equation (Eqn. 3.1) the $\tau_r$ values can be related to the volumes of the observed species (Table 3.2). These volumes suggest that the medium fraction is a pentamer or hexamer, the slow fraction a 15-18 mer.

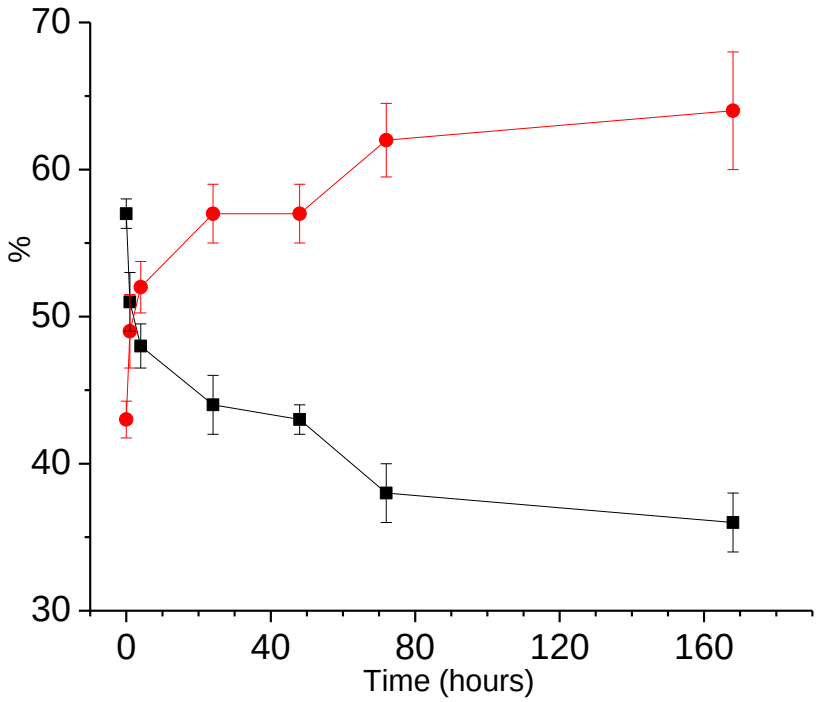


***Figure 3.4*** *Aggregation of T0EZ as a function of time. Amount of aggregates (red, slow and medium EPR components combined); amount of monomers (black, fast EPR component). The lines are a guide to the eye.*

Figure 3.4 shows that the amount of combined slow and medium component increases for the first 70 hours of aggregation, afterwards it stays constant within the error margins, indicating that a steady state is reached. Also at the earliest time points some aggregates are present.

***Table 3.3*** *The rotational correlation times of the monomers of T0EZ, T5EZ and T12EZ. Molecular volumes ($V_{MW}$) monomers calculated from the molecular weight (MW) using the protein density equation (Eqn. 3.2).*

| Peptides | $\tau_R$ Monomers [ns] | $V_{EPR}$ [nm$^3$] | $V_{MW}$ [nm$^3$] |
|---|---|---|---|
| **T0EZ** | 0.16 ± 0.004 | 0.65 ± 0.02 | 1.78 ± 0.17 |
| **T5EZ** | 0.40 ± 0.02 | 1.61 ± 0.07 | 1.65 ± 0.15 |
| **T12EZ** | 0.31 ± 0.02 | 1.25 ± 0.06 | 1.78 ± 0.17 |

Finally, in Table 3.3, the $\tau_r$ values of all TOAC-EZ constructs in their monomeric state are given. The peptides T0EZ and T12EZ have the same composition, T5EZ has one amino-acid residue less. Thus from the volume of the peptide one would expect that T0EZ and T12EZ have longer $\tau_r$ values than T5EZ, however the opposite is true. This suggests that the TOAC in T0EZ and T12EZ has residual freedom to move making the observed $\tau_r$ shorter than expected from the molecular weight.

# 3.4 Discussion

In this study we use cw, room temperature EPR at 9 and 95 GHz to determine the size-development of amyloid oligomers in time. The size of the aggregates can be tracked in situ, in the aggregation solution. The method is demonstrated with an amyloid peptide based on K11V[67] into which we incorporated the backbone-fixed spin label TOAC.

## *3.4.1 Is TOAC a good monitor for peptide size?*

Even though TOAC is directly linked to the peptide backbone (Figure 3.1d), local backbone motion could still uncouple it partly from the peptide-oligomer-overall rotation. To assess this factor we consider the $\tau_r$ values for the monomeric peptides (Table 3.3). The $\tau_r$ values are related to the volume of the object via the Stokes-Einstein relation (Eqn. 3.1) resulting in $V_{EPR}$. This volume is compared to the molecular volume of the peptides obtained from the molecular weight (Eqn. 3.2), $V_{MW}$. In Table 3.3 these volumes are given. For T5EZ, $V_{EPR}$ is close to the $V_{MW}$, showing that for this peptide, $\tau_r$ is a good measure for the peptide size. The peptides T0EZ and T12EZ have smaller $V_{EPR}$ values than T5EZ, although their molecular volumes are larger. This shows that the motion of the spin label at the N- and C-terminus is partially uncoupled from that of the peptide, in other words, the backbone section that the TOAC is attached to displays local mobility. Comparing all three peptides, the mobility is higher at the N-terminus than at the C-terminus (T0EZ has a shorter $\tau_r$ than T12EZ), and smallest in the center (T5EZ). The case of T5EZ shows that the concept of using TOAC to monitor the molecular volume works well, at least in a situation where the TOAC is well embedded in the object. The $\tau_r$ values of all TOAC constructs are longer than those of the MTSL analogues, see SI Table S3.2, as expected, given that in MTSL the nitroxide is not rigidly linked to the protein backbone.

## *3.4.2 Influence of TOAC position on the aggregation of the EZ peptides*

Two of the three TOAC constructs (T5EZ and T12EZ) do not aggregate. For T5EZ, with the TOAC in the middle of the β-sheet region, two factors combine to inhibit aggregation: Crowding in the middle of the β-barrel (see Figure S3.3) and the α-helix-inducing properties of TOAC, which could inhibit the formation of the β-sheet and thereby of the oligomer. To test whether the α-helix-inducing character of TOAC is the dominant factor inhibiting aggregation, we also tested the MTSL-labelled counterparts (see SI). Also, the

equivalent constructs to T5EZ and T12EZ with an MTSL label failed to aggregate. As MTSL labels do not break β-sheets, it seems evident that crowding is more important than β-sheet breaking. More puzzling is the question why the TOAC at the C-terminus inhibits aggregation, whereas at the N-terminus it does not. Here the difference in the $\tau_r$ values of T0EZ and T12EZ could give a hint. Apparently, the N-terminus has a higher local mobility than the C-terminus, and that, in turn, may enable TOAC at the N-terminus to avoid molecular crowding in the oligomer, enabling T0EZ to aggregate to oligomers.

### *3.4.3 Oligomerization of T0EZ as followed by EPR*

Having established that TOAC enables to track molecular size, i.e. the number of peptides per oligomer, we use it to analyse the aggregation of T0EZ. The size and the amount of the oligomers increases with time (EPR) (Figure 3.4 and S3.2), the aggregates have β-sheet structure (CD) and do not convert to fibrils on the time scale of the experiment (ThioT). With respect to the size of oligomers, an initial fraction of smaller oligomers (medium fraction by EPR), some of them present even at the earliest time point taken, and a later fraction with larger aggregates (slow fraction) are observed (Figure S3.2). These are two distinct populations, as two spectral components, the medium and the slow, are needed to represent them. The number of monomers in the two fractions, penta-to-hexamers and 15-18 mers (see Table 3.2), has a large uncertainty as several approximations enter in the estimation. In the SI these are described and evaluated quantitatively. The impact of some approximations can be determined quantitatively: The two different ways to estimate monomer volumes (Table 3.2), show that for the smaller oligomers (medium EPR fraction) differences of one monomer unit and for the larger oligomers (slow EPR fraction) differences of three monomer units result. Other factors can be qualitatively assessed: The local mobility of the TOAC in the oligomer leads to an underestimation of the size of the oligomer, thus the oligomer size determined by is a EPR a lower limit (for details, see SI). Overall, due to the approximations described in the SI, the relative oligomer sizes are more reliable than the absolute values. To determine the absolute number of monomers in the oligomers, dedicated experiments are possible (see below).

The oligomers are most likely heterogeneous, i.e. the two oligomer fractions do not consist exclusively of oligomers of one particular size. A homogeneous population would have a distinctive lineshape as shown in Figure S3.6, and it is likely that also the superposition of two homogenous populations would still give spectra that are better resolved than those experimentally observed. More detail could be obtained by increasing the time resolution, i.e. by measuring more time points. Such experiments could also reveal, if the oligomers grow by adding monomers or whether smaller oligomers assemble into the larger ones, however such experiments are beyond the scope of the present study.

Additional EPR experiments could determine the number of monomers in specific oligomers[114,115], as an independent check point, however, these methods rely on frozen solutions and thereby lack the power of the in situ measurement we present here.

## *3.4.4 Aggregation of T0EZ*

The investigation presented gives clear evidence that the aggregation of T0EZ proceeds in several steps. It reveals an initial fraction, the EPR medium fraction, which, considering the approximations described in the SI, may be an hexamer similar to that observed by Laganowsky et al.[67]. The β-barrel structure is confirmed by CD, its hexameric nature fits well with the rotation correlation time derived from EPR. The exact shape, e.g. the antiparallel arrangement of the peptides (Figure 3.1) would have to be confirmed by more extensive EPR investigations, see below. While these oligomers are the end point of aggregation under the conditions employed in Laganowsky et al.[67], the present study shows a further growth of the aggregates over time, to larger oligomers, as proven by the size observed by EPR (15 – 18 peptides). The absence of ThioT activity rules out that these latter objects are fibrils, in particular, it shows that the oligomers do not have the non-curved β-sheets required for ThioT binding. Laganowsky et al. show that K11V forms fibrils when exposing it to vigorous shaking at 50 $^{0}$C over a period of 7 days. The lower temperature of the present experiments was chosen to enhance oligomers, therefore, in the present study, high temperature and vigorous shaking were avoided. Our finding of two different types or groups of oligomers that differ in size suggests that the respective oligomers can have different physiological/disease effects and that their properties must be studied individually for a full understanding of their relevance.

Also other studies have shown that oligomers can increase in size over time[116,117]. In particular, ion-mobility mass spectrometry (IM-MS) showed that other short amyloid peptides, when investigated under conditions that are not optimized for crystallization also go through a series of oligomers, the size of which increases over time.[118,119]

Overall we observe the aggregation of T0EZ into oligomers with a β-sheet structure. The absence of ThioT fluorescence confirms that, at least within the time scale investigated (12 days), no fibrils are formed. Therefore, these oligomers are unlikely to be seeds for fibrilization and should be considered off-pathway oligomers. More detail could be determined by kinetic analysis as pioneered by the Knowles group[117]. The approach of the present study is of course not limited to this particular peptide: Other short peptides, especially those that aggregate to fibrils, could be investigated. In these cases, besides the end-product, the fibrils that should be ThioT active, on- and off-pathway oligomers are expected. To compare the properties of these oligomers to those occurring in the EZ oligomers would give further insight into the aggregation process that from the physical-chemistry point of view is still far from understood.

## 3.5 Conclusions and outlook

Here we show that peptides with TOAC at strategic positions combined with high-field EPR open a new way to study amyloid aggregation: The real-time measurement of rotational motion reveals directly the size of the oligomer at specific time points. While, in the model system we investigate, only two chief fractions are observed that differ by approximately 12 monomers, the approach itself can follow the development with single-monomer resolution in the otherwise difficult to differentiate[43] oligomer size distribution from two to 15 monomers, see SI. Our approach is therefore one of the few methods presently available to track oligomers as they develop. In contrast to IM-MS, a method that provides the molecular mass and information about the outer size of the oligomers after gas-phase ionization, the high-field EPR approach presented here determines the oligomers in solution, avoiding chemical separation, vacuum-desorption and gas-phase, ionization steps. It therefore perfectly complements existing methods and is an excellent new tool in in the quest for molecular information on amyloid aggregation. We show here that the approach can be applied to one particular peptide, however, the principle shown is universal for other peptides of interest, as long as they are amendable to SPPS to incorporate the TOAC, either for the full peptide or a fragment that can be fused to a protein that provides the full-length sequence of interest. We also demonstrate that in spite of adverse properties of TOAC, aggregating peptides can be generated. Of course, the presence of TOAC and its eventual effects on the aggregation should be tightly monitored. These disadvantages clearly are outweighed by the merits of the TOAC approach, as can be seen in the poor size differentiation obtained from the conventionally labelled peptides in the SI.

Finally, once the intermediates are identified and their size development over time is established by the approach presented here, the structure of each of the identified states can be investigated: By distance determination using EPR via spin-spin interaction[58] and other techniques, inter- and intramolecular interactions can be determined, yielding structural constraints for modelling. Small angle X-ray scattering (SAXS) can identify overall shape, CD and FTIR can yield internal structure.

Furthermore, for many systems the present detail would already yield new insights: On- and off-pathway oligomers could be tracked in their time development[97]. These experiments would identify states that warrant more detailed investigation such as determining their individual mode of toxicity and applying further structural methods.

# 3.6 Supporting information

## *3.6.1 Supplementary figures*

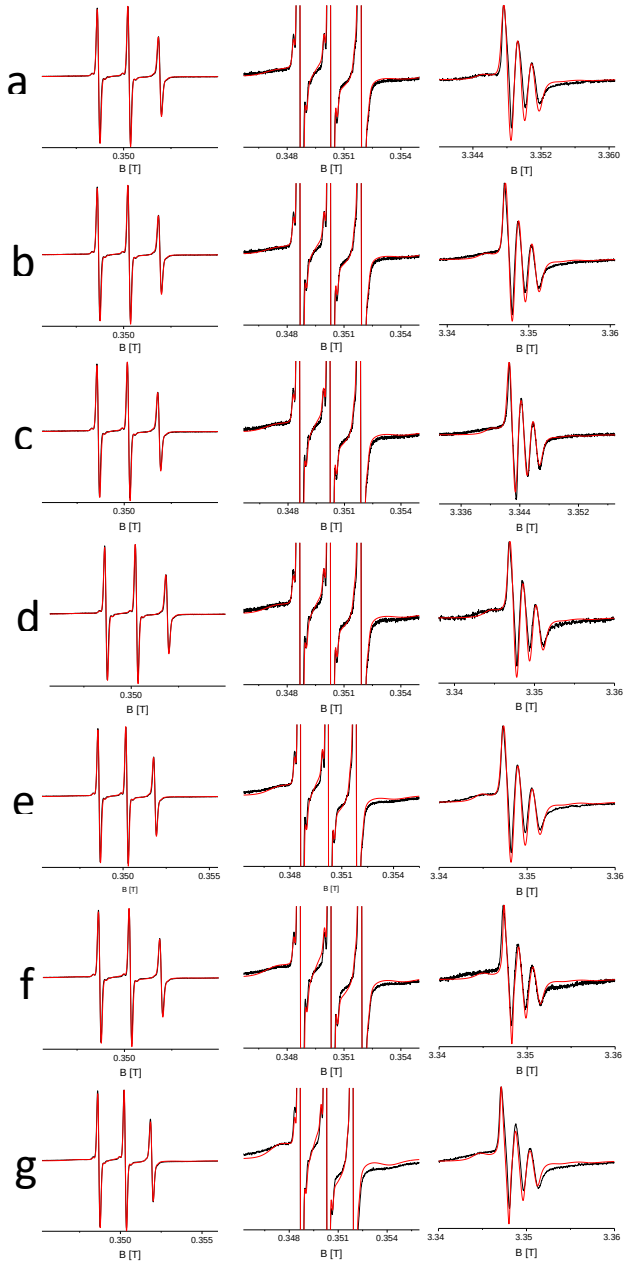


***Figure S3.1*** *Room temperature 9 and 95 GHz EPR spectra of T0EZ for the entire time point series taken during aggregation. Left: 9 GHz EPR, full spectra. Central: 9 GHz EPR spectra, amplitude expanded ten-fold. Right column: 95 GHz spectra. Spectra a) 0 hrs, b) 1 hr, c) 4 hrs, d) 24 hrs, e) 48 hrs, f) 72 hrs, g) 168 hrs. Black: Experimental spectra. Red: Simulated spectra. Remaining experimental conditions and detailed description: See main text.*

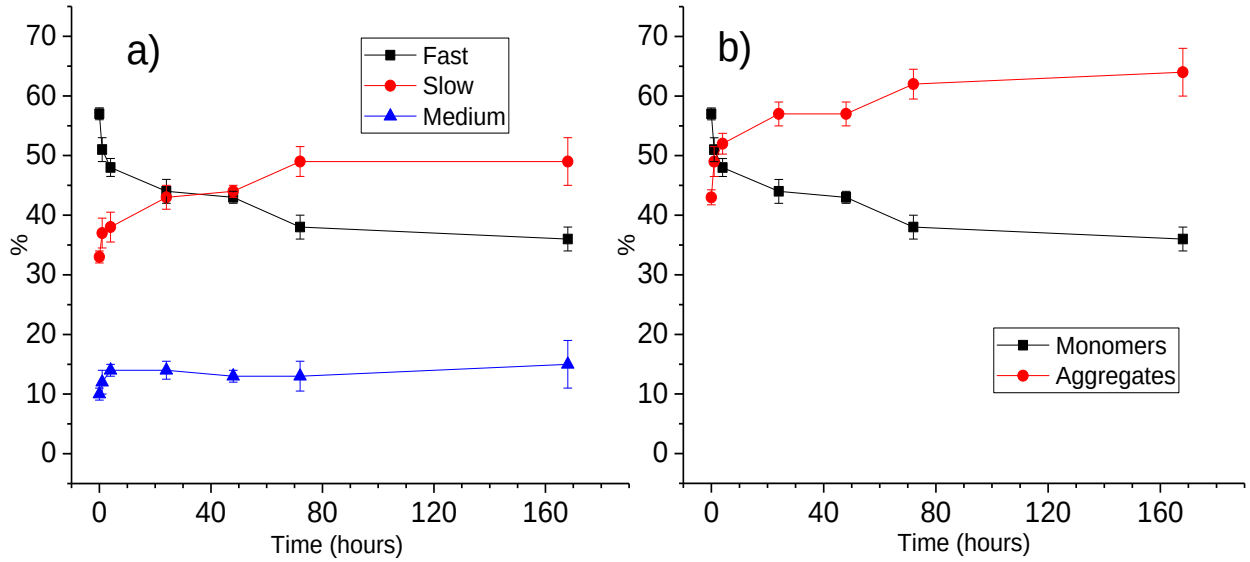


***Figure S3.2*** *a) Amount of the fast, medium and slow components in the EPR spectra of T0EZ as a function of the aggregation time: fast (black), medium (blue) and slow (red). b) From Figure 3.4 in the main text: Slow and medium components combined (red). The lines are a guide to the eye.*

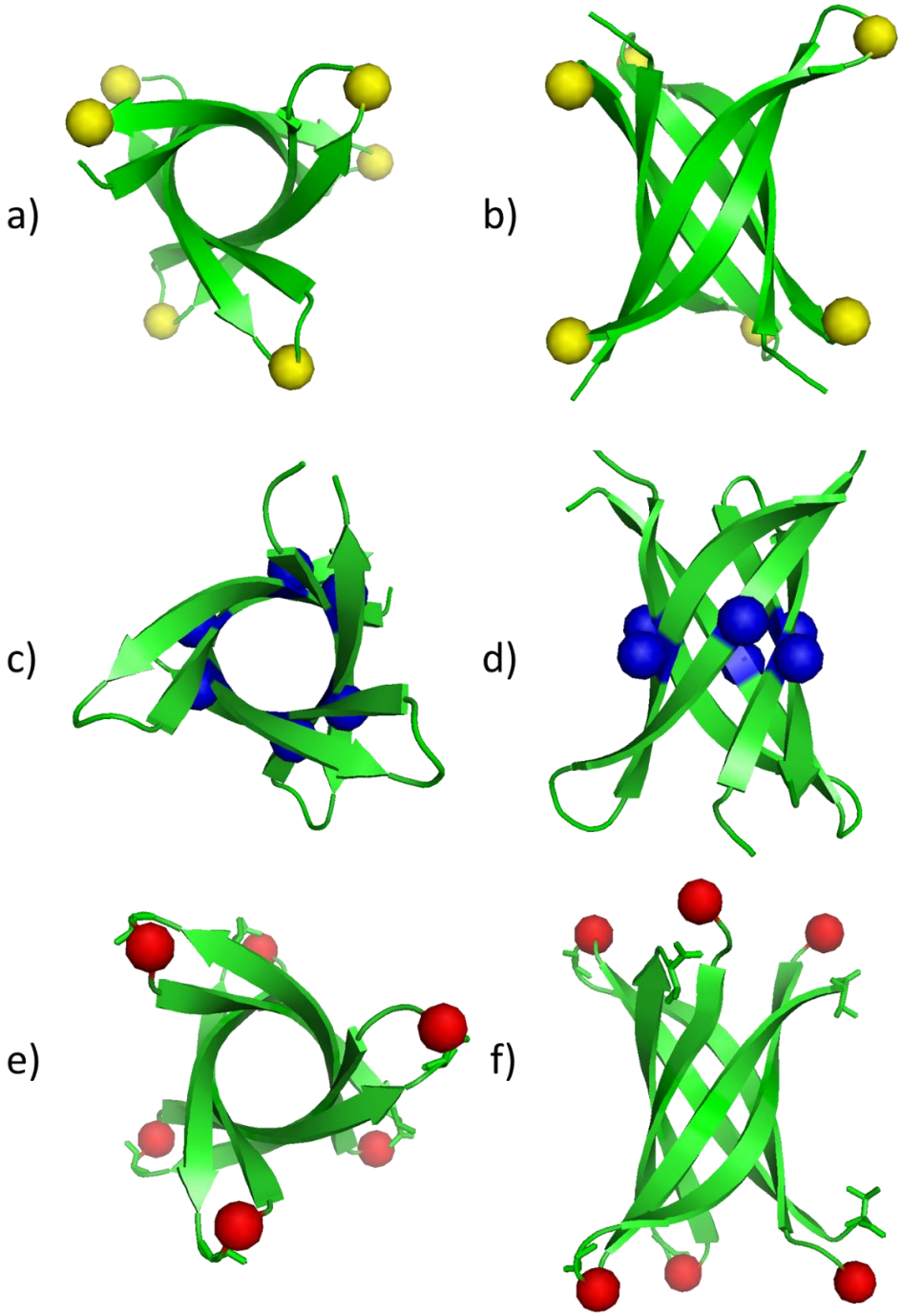


***Figure S3*** *Location of TOAC spin label expected for T0EZ, T5EZ and T12EZ, given the structure of the K11V oligomer (PDB 3SGO)*[67]*. a) T12EZ-TOAC: yellow spheres. b) view in a) rotated by 90º. c) T5EZ-TOAC: blue spheres. d) view in c) rotated by 90º. For reference also for T0EZ, the TOAC location is shown: e) T0EZ-TOAC: red spheres. f) view in e) rotated by 90º, see also Figure 3.1a) and b).*

## 3.6.2 Supplementary materials and methods

### 3.6.2.1 Circular dichroism

The CD spectra were obtained using a J-815 CD Spectrometer (Jasco Benelux, Utrecht, The Netherlands). The measurements were carried out at room temperature under the conditions of 260 nm - 190 nm wavelength range, continuous scanning mode, a band width and a data pitch of 1 nm each, a speed of 20 nm/min and a total of five accumulations for each measurement. The 40 µL samples for each aggregation time point were diluted ten times in milli-Q water. A 2-mm-path-length cuvette was used for measurements.

## 3.6.3 Supplementary data

### 3.6.3.1 Circular dichroism of T0EZ aggregation

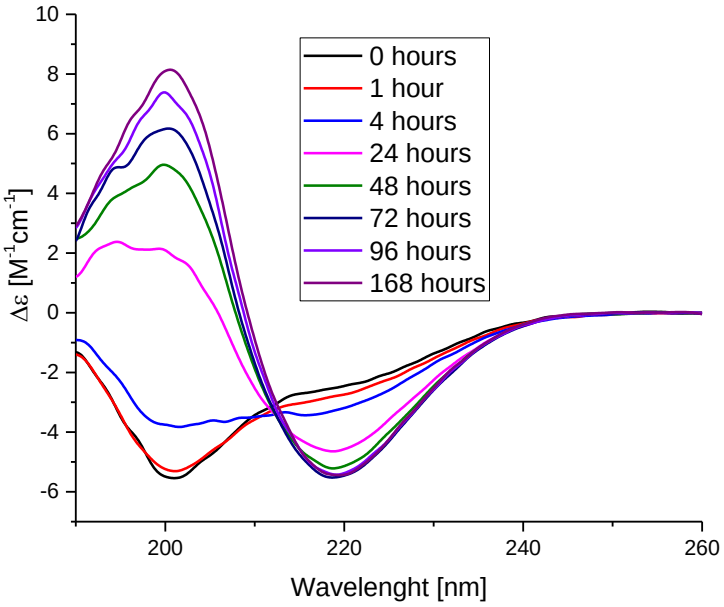


***Figure S3.4*** *Development of the CD spectra of T0EZ measured at different time points of aggregation at room temperature. The spectra have been smoothed by 15 points FFT filter by Origin® for better visualization. At time zero the spectrum (black) presents a lineshape of a random coil structure. After 168 hours the spectrum (wine) shows a lineshape of a β-sheet secondary structure.*

Figure S3.4 shows the T0EZ circular dichroism (CD) spectra measured over the time course of aggregation. In Figure S3.4 there is a gradual progression of the lineshape from random coil to a β-sheet configuration. The negative feature at 200 nm, characteristic for random coil, becomes positive through time which is a sign of β-sheet structure

formation. The negative peak with increasing amplitude around 218 nm is also characteristic of β-sheet. The development suggests an increase of β-sheet character over time, which is expected for β-sheet oligomers.

To obtain the secondary structure composition of the sample according to the CD spectra we use the BeStSel program designed to decompose the CD spectra of proteins. Figure S3.5 shows the results for the 190 nm to 260 nm wavelength range. As CD averages the secondary structure per residue over time whereas EPR yields the composition per peptide, a 1 : 1 correspondence of the percentage contribution cannot be expected. Nevertheless, the methods show the same trend: Decay of random coil (CD) and monomer content (EPR) and an increase in β-sheet (CD) and oligomers (EPR). Numerically, random coil and EPR fast fraction agree for the samples up to 20 hours, after that the agreement is better when the random coil and turn fractions from the CD analysis are added. The model of K11V predicts anti-parallel arrangements of the strands in the K11V oligomer, so the parallel β-sheet component in the CD analysis is surprising. As also the attribution of secondary structure elements in CD spectra within BeStSel is not completely established, additional structural information about the species occurring during oligomerization would be needed to clarify this point. Distance measurements by EPR[59,120,121] could provide this kind of information, however, it is beyond the scope of the present investigation.

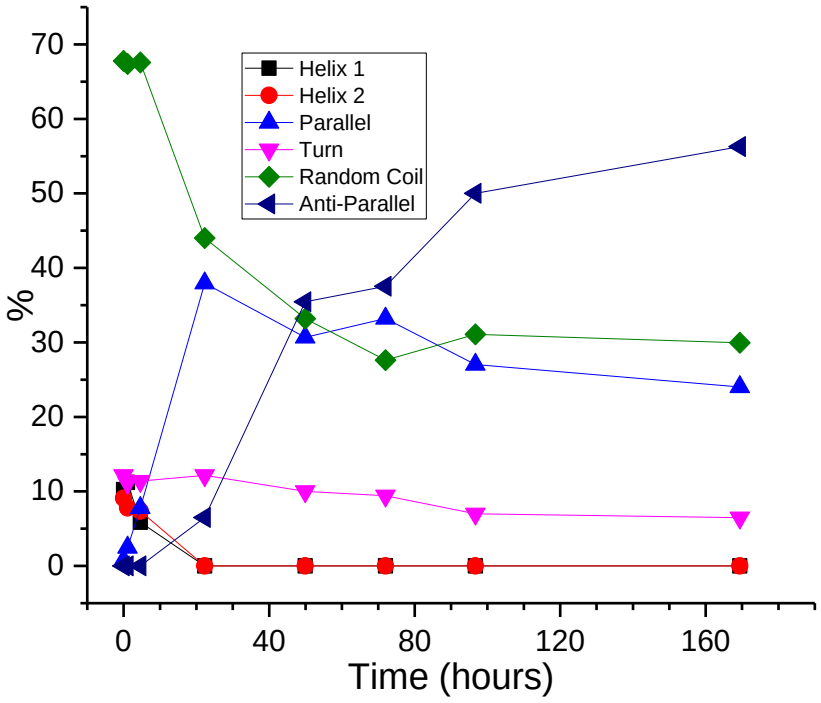


***Figure S3.5*** *Analysis of the CD spectra in Figure. S4 using BeStSel software[111,112], showing the amount of the secondary structures of T0EZ over time derived from the CD spectra. Helix 1 (black) and helix 2 (red) are the different helical conformations. Random coil (green) is considered as mainly being the "Others" component of BeStSel. BeStSel provides three antiparallel β-sheet components, left-twisted (Anti1), relaxed (Anti2) and right twisted (Anti3), which are added up here as Anti-Parallel (navy). For the first 4 hours, when Anti1 and Anti2 were zero, the value of Anti3 (having a basis spectrum similar to that of the disordered structure), was added to the random coil. Parallel (blue) is the parallel β-sheet structure. Turn (pink) is the beta-turn structure. The lines are a guide to the eye.*

### *3.6.3.2 Activity of TOAC and diamagnetic dilution*

Low spin label activity in peptides results in diamagnetic dilution. Protonation by strong acids (TFA) used during peptide synthesis to cleave the peptide from the resin (see Materials and Methods) is known to reduce and thereby inactivate the nitroxide of TOAC at least partially[84].

Two experiments show that this is also the case for T0EZ: The concentration of the peptide determined from the weight of the lyophilized powder is five times higher than the spin concentration determined by EPR, as described in Materials and Methods, showing that only 20 % of the TOAC is active in the peptide. To confirm that TOAC is inactivated by TFA, a sample of T0EZ in DMSO was incubated for 3 hours by adding 10 % of a solution of $NH_3$ in water (Sigma-Aldrich 28-30 %). After incubation, the EPR signal had increased by a factor of four, confirming that acid-deactivation by TFA is the most likely origin of low spin concentration of the as-synthesized T0EZ.

While usually undesired, here we use the as-synthesized T0EZ without activation because the low activity of TOAC provides a convenient – and otherwise difficult to realize – way to diamagnetically dilute spins. During aggregation the peptide with a paramagnetic, active TOAC will be incorporated randomly with the inactive peptides into the aggregates, which is referred to as diamagnetic dilution. Diamagnetic dilution increases the spin-spin distance, generating spectra devoid of spin-spin interactions, if (i) the ratio of inactive vs active labels is sufficiently large considering the expected distance and (ii) if the species with active spin labels are randomly distributed in the structure.

$$z = \frac{n!}{(n-p)!\,p!} \cdot a^p \cdot (1-a)^{n-p} \qquad (S3.1)$$

To estimate if condition (i) is fulfilled, we analyze the spin proximity in the cylindrin hexamer.[67] Eqn. S3.1 defines which fraction of hexamers $z$ contains a given number $p$ of active TOAC labels. In Eqn. (S3.1) $z$ is the population of spin-labelled oligomers, $p$ is the number of active spin labels in the oligomer, $n$ is the number of monomers in the aggregate and $a$ is the fraction of active spin labels.

For a $p$ of 2 Table S3.1 shows that 26 % of the hexamers are expected to contain two labeled peptides. In this fraction the distances between the two spin centers is expected to be either 15 Å or 25 Å[67]. This corresponds to a dipolar interaction of 2.45 MHz and 0.53 MHz, i.e. 0.09 mT to 0.02 mT. Such a broadening would be undetectable given the width of the spectral lines, allowing us to neglect any influence of spin-spin interactions in the analysis. A random distribution of active and inactive peptides (assumption (ii)) is likely as both types of peptides only differ in the protonation state of the nitroxide, so they have almost identical chemical structures.

***Table S3.1*** *Number of spin-labelled peptides with active nitroxides expected for hexameric oligomers.*

| *p* | *z* % |
|---|---|
| 0 | 23.0 ± 2.0 |
| 1 | 38.0 ± 3.0 |
| 2 | 26.0 ± 2.0 |
| 3 | 9.8 ± 0.8 |
| 4 | 2.0 ± 0.2 |
| 5 | 0.2 ± 0.1 |

### *3.6.3.3 Simulations of EPR spectra: Quality of the fits*

As described in the main text, the overall strategy was to simulate the spectra with a common set of parameters, using the smallest number of components that fit the entire time series, to avoid overfitting the data. Here we discuss this approach in more detail and describe its consequences for the simulations. Three components, the fast, medium and slow, were sufficient. For each individual time point, the 9 and 95 GHz EPR spectra were fitted with the same composition of these three components, finding the optimum that agrees best for both spectra. Relaxing these constraints or introducing other mobility models, such as anisotropic rotation models[122–124], improves the simulation of the individual spectra, but introduces additional parameters that may result in overfitting the spectra. The results of the three-component simulations are displayed in Figure S3.1, in which the simulated spectra are shown in red. For aggregation times up to 24 hours, the agreement of simulation and experiment is very good for 9 and 95 GHz spectra, whereas later time-point spectra show some deviation: As a representative for deviations, we discuss the spectra in Figure S3.1f): The experimental 95 GHz spectrum has intensity at the low field side of the spectrum ($B_0$ = 3.340-3.345 T) and the high field side of the spectrum ($B_0$ = 3.353-3.357 T) that is not covered by the simulation. This spectral intensity would correspond to a very slow/immobilized component in the spectrum that is not compatible with the 9 GHz EPR spectrum. The appearance of such a slow component in the 95 GHz spectra could derive from instrumental effects: The overall baseline stability in 95 GHz EPR is worse than in 9 GHz, so part of this broad component could be attributed to such instabilities. They would have a stronger impact on the later time spectra, because the amplitude of the narrow, three-line spectrum is less, causing an apparent increase in amplitude of baseline artefacts (note that in Figure S3.1 the spectra are amplitude scaled to the narrow component). Secondly, the samples for 95 GHz EPR had to be stored frozen before the measurements, whereas most of the 9 GHz EPR spectra were measured directly after the samples were drawn from the aggregation mixture. It cannot be excluded that freezing affects the sample. We therefore considered this spectral intensity in the 95 GHz EPR spectra as less important and focused more strongly on the 9 GHz EPR spectra of this particular time point. Apparently, for this time point the

optimum solution for both 9 and 95 GHz EPR spectra limits the degree of agreement of simulation and experiment that can be reached.

### *3.6.3.4 Comparison of $\tau_r$ in TOAC versus MTSL-labelled EZ peptides*

***Table S3.2*** *Experimentally determined rotational correlation times of monomeric EZ peptides from 9 GHz and 95 GHz EPR. MXEZ: construct with MTSL at the same position as the TOAC in TXEZ. Molecular volumes from EPR ($V_{EPR}$) and molecular weight ($V_{MW}$) are also given (see main text).*

| Peptides | $\tau_R$ Monomers [ns] | $V_{EPR}$ [nm$^3$][a] | $V_{MW}$ [nm$^3$][b] |
|---|---|---|---|
| **T0EZ** | 0.16 ± 0.004 | 0.65 ± 0.02 | 1.78 |
| **T5EZ** | 0.40 ± 0.02 | 1.61 ± 0.07 | 1.65 |
| **T12EZ** | 0.31 ± 0.02 | 1.25 ± 0.06 | 1.78 |
| **M0EZ** | 0.14 ± 0.01 | 0.56 ± 0.03 | 1.89 |
| **M5EZ** | 0.18 ± 0.003 | 0.73 ± 0.01 | 1.69 |
| **M12EZ** | 0.15 ± 0.004 | 0.59 ± 0.02 | 1.89 |
| **K11V** | | | 1.47 |
| **EZ** | | | 1.61 |

a) From Stokes-Einstein (Eqn. 3.1).
b) From protein density (ρ = 1.35 g/cm$^3$) (Eqn. 3.2).

Table S3.2 gives the values of $\tau_r$ of the monomeric EZ peptides obtained from the simulations of the 9 GHz and 95 GHz EPR spectra. In addition to the values for T0EZ, T5EZ and T12EZ (Table 3.3 main text) also values for the MTSL-labelled EZ peptides are given. The MTSL-EZ peptides contain the spin-labelled cysteine at the N-terminus (M0EZ), at position 5 (M5EZ) and at position 12 (M12EZ), for sequences see Table 3.1 in the main text. All MTSL-constructs have shorter $\tau_r$ than the TOAC counterparts, reflecting a higher local mobility of the MTSL label than the TOAC label. The difference in $\tau_r$ is largest for T5EZ and M5EZ. The $\tau_r$ value for T0EZ is half of that of T12EZ, as discussed in the main text. This shows that the backbone mobility is higher at the N-terminus than at the C-terminus of the EZ peptide. The rotational correlation times of M0EZ and M12EZ are the same within the experimental error, showing that local mobility, i.e. rotation about the single bonds linking the nitroxide to the backbone, masks backbone-mobility differences.

We tested the MTSL-labelled peptides for aggregation the same way as for the TOAC counterparts. The M0EZ peptide aggregated similarly to T0EZ. Similar to T5EZ and T12EZ, also M5EZ and M12EZ failed to aggregate. As MTSL labels do not break β-sheets, this finding shows that the inhibition of aggregation from crowding of the spin labels is more important than β-sheet breaking propensity of the TOAC.

## *3.6.3.5 Approximations used in oligomer size estimation*

As described in the main text, the Stokes-Einstein relation establishes that $\tau_r$ is proportional to the volume of the aggregate and, together with the protein density, it gives an estimate for the number of monomers in the aggregate. Utilizing this approach involves several approximations, the impact of which we describe in the following. Some of these approximations can be tested against the known structure of one of the oligomers expected for the EZ peptides: The hexamer cylindrin[67]. For this oligomer the X-ray structure is known and the rotational correlation times can be calculated from first principles by HYDRONMR[125].

***Table S3.3*** *Size of oligomers from different methods and effects of approximations. Number of monomers in oligomer $n_i$ and rotational correlation times ($\tau_r$) are also given.*

| | | | method (i) | | method (ii) |
|---|---|---|---|---|---|
| **EPR component** | **$\tau_r$ from EPR [ns]** | **$\tau_r$ from HYDRONMR [ns]** | **$\rho$ = 1.35 g/cm$^3$** | **$\rho$ = 1.50 g/cm$^3$** | |
| **medium** | 2.00 ± 0.20 | 5.78[a)] | 4.52 | 5.03 | 5.81 |
| **slow** | 6.31 ± 0.70 | n.a. | 14.27 | 15.88 | 18.31 |

a) $\tau_1$ = 4.96 ns; $\tau_2$ = 6.20 ns; $\tau_3$ = 6.16 ns

### *Influence of protein density on values of $n_i$ (method (i))*

The protein density impacts $n_i$ as seen in Table S3.3, comparing the two columns headed method (i). A value of $\rho = 1.35$ g/cm$^3$ (left column) is generally accepted for typical folded proteins (MW $>$ 20 kDa)[110] yielding the parameters that are also given in the main text, however, for proteins with progressively smaller MW, the density is increasing due to a larger relative impact of the hydration shell at lower protein volumes[109]. Thus a larger density ($\rho = 1.5$ g/cm$^3$) appears appropriate under some circumstances, and the resulting values are given in the right column[110]. Comparing the two columns, the oligomer sizes differ by 0.5 (medium fraction), resp. 1.5 (slow fraction) monomer units, showing that for the medium fraction the size approaches a pentamer. As the slow EPR fraction suggests a molecular weight of 23 kDa, the higher density does not seem appropriate for that fraction, showing that $n_i$ for that fraction should be closer to a 14-mer than a 16-mer.

### *Using monomer volume for cylidrin (method (ii))*

Method (ii) uses the volume of the monomer derived from the volume of the hexameric oligomer as obtained from x-ray crystallography[67]. It does not require the protein density. It results in a hexamer for the medium and a 18-mer for the slow fraction.

***Influence of the spherical approximation on $n_i$***

The Stokes-Einstein relation (Eqn. 3.2, main text) implies a spherical object. For non-spherical objects the volumes derived from the Stokes-Einstein relation do not reflect the volume of the object accurately, as described here. Also, the lineshape of the EPR spectra can show systematic variations from those of a spherical object, and rather than by a single $\tau_r$, the isotropic $\tau_r$ ($\tau_0$), the anisotropic $\tau_r$ values $\tau_1$, $\tau_2$ and $\tau_3$ should be used.

The impact of any deviation of the shape of the oligomers from a sphere on the volume is estimated considering the theory of axially symmetric rotational ellipsoids. Axially symmetric rotational ellipsoids are described by the axis system *a, b, c*, where *a* is the semi-axis along the symmetry axis and *b* and *c* are perpendicular to it. For a > b, a prolate, and for a < b, an oblate ellipsoid results. The relation between $\tau_r$ and the volume of such particles is described by Perrin et al.[126], Koenig et al.[127] and summarized by Marsh and Horvath[128]. For cylindrin[67], where the radius of the cylinder (11 Å) is equal to the half-height of the cylinder (total height 22 Å), b/a = 1 results and Figure 1 of Koenig[127] shows that $\tau_1$, the rotation correlation time about the symmetry axis *a,* is 1.4 times larger than $\tau_r$ of a sphere of the same volume ($\tau_0$). Along the two equivalent axes $\tau_r \approx \tau_0$. The averaged $\tau_r$ for such an ellipsoid could therefore be 1.3 times longer than that of a sphere. Thus the volume of the cylindrical ellipsoid would be 1.3 smaller than that of a sphere. For the smaller oligomers (medium $\tau_r$ fraction from EPR) the number of monomers in the oligomers would reduce from five to four. The effect of other aspect ratios on $\tau_r$ can be obtained from Figure 1 in Koenig[127]. In all cases, the $\tau_r$ values of non-spherical objects are larger than those of a sphere of equivalent volume, suggesting a systematic over-estimation of the particle size in the spherical approximation. As the anisotropy of the rotation should be visible in the EPR spectra, EPR experiments at higher field/frequency values would help to determine the degree of anisotropy. Such experiments are beyond the scope of the present study.

***Influence of local mobility on oligomer size***

If the motion of the nitroxide is faster than that of the oligomer, the oligomer size determined by $\tau_r$ would be smaller than the real value, an effect referred to as local mobility of the nitroxide. For proteins labelled conventionally with the MTSL label, Figure 3.1d, this is a severe problem. The nitroxide TOAC, Figure 3.1c, is part of the protein backbone, which will suppress local mobility effects considerably. The $\tau_r$ of one of the EZ peptides (T5EZ) matches its volume (see Tab 3.3, main text) showing that local mobility at the center of the peptide is negligible, also, this $\tau_r$ is significantly longer than that of M5EZ, emphasizing that the $\tau_r$ of TOAC peptides is more closely correlated with the size of the object than for peptides labelled with MTSL. As described in the main text, the N-terminus of T0EZ must be somewhat flexible, so we cannot exclude that the size of the oligomer is somewhat underestimated. We are not aware of studies that have quantitatively analysed this point, in contrast to the situation for MTSL where extensive studies were performed by the Hubbell group[47,129–133].

***Hydrodynamic simulations by HYDRONMR***

For K11V, the structure of one oligomer is known, so the $\tau_r$ value for this structure can be calculated by HYDRONMR. The obtained $\tau_r$ values give insight into the anisotropy of the rotation and absolute $\tau_r$ values for the hexamer. In Tab. S3.3 these values are given: the anisotropy is relatively small and agrees well with an axially symmetric prolate object. The absolute isotropic $\tau_r$ value is longer than calculated by methods (i) and (ii). Clearly , HYDRONMR provides a more realistic representation of the structure of the oligomer and of the hydration layer. The empirically derived protein densities take hydration into account, however, without considering the surface details of the protein and methods (i) and (ii) imply spherical approximation. The impact of the respective approaches for oligomers of the type observed here are difficult to assess. We observe that the $\tau_r$ of the hexamer cylindrin from HYDRONMR is significantly longer than that of the medium fraction. There are two possible interpretations: Either, the medium fraction is due to a smaller oligomer than the cylindrin, or the faster $\tau_r$ value observed experimentally is due to local mobility.

***Final assessment***

As far as the effect of the approximations of the approaches described can be quantified, the errors introduced are 1-1.5 monomer units per oligomer (e.g. method (i)). Some approximations lead to systematic deviations: Deviation of the oligomer from a sphere causes the oligomer size to be overestimated, local mobility causes the opposite effect and one could hope for some cancellation of errors. Conservatively, an estimate of 2-3 monomers units results for the absolute number of monomers in the oligomers, however, as several factors causing these uncertainties may be similar for some or all oligomers, relative sizes are more reliable and qualitative size distinctions can be made. In the main text, Discussion section, specialized experiments based on pulsed EPR and other techniques are described that can determine accurate oligomer sizes, however, most of these cannot be applied in situ. The present approach provides the overview of the entire aggregation process and can identify states of interest, e.g. how many distinct oligomer states there are, and what the relative sizes of oligomers are. Once established, these states can be investigated more quantitatively by the methods referred above.

### *3.6.3.6 Can single monomer resolution of oligomer size be attained?*

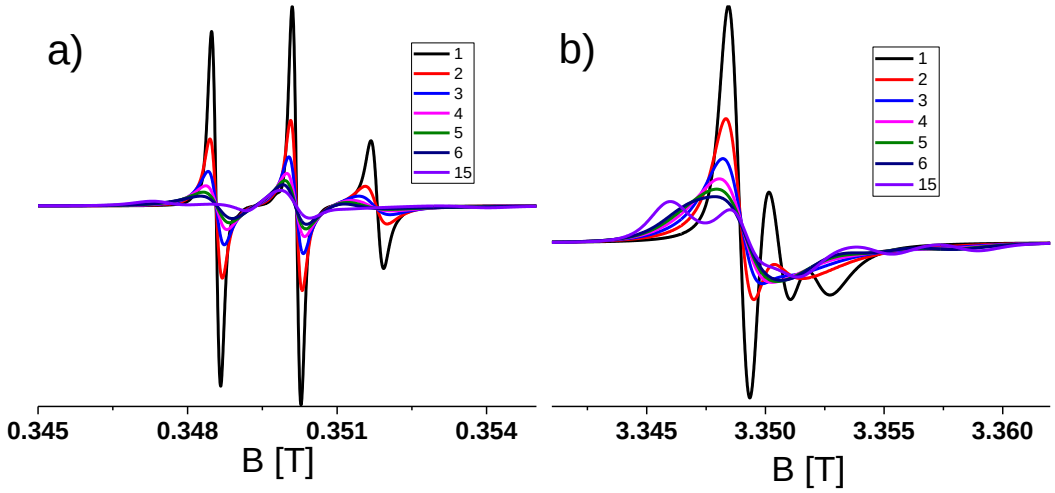


***Figure S3.6*** *Simulations of EPR spectra of T0EZ for the expected volumes of different sized oligomers, one monomer at a time. The $\tau_r$ values were calculated based on the $V_{MW}$ using the same parameters as for the simulations of the experimental spectra (see Material and Methods in the main text). a) Simulations of 9 GHZ spectra of a molecule with rotational correlation times ranging from 1.8 ns (black) to 26.7 ns (purple). b) Simulations of 95 GHZ spectra for the same rotational correlation times.*

Figure S3.6 shows the 9 GHz and 95 GHz EPR spectra expected for oligomers of different sizes in single-monomer increments. Sizes range from 1 to 15 mer aggregates. Peptide volume used: $V_{MW}$ of T0EZ. Especially in the 95 GHz EPR spectra, the differentiating power of the method is high: Monomers are clearly set off from dimers, and up to hexamers individual species can clearly be distinguished in the low- and high-field region of the spectra. Similarly, resolving oligomers from hepta- to 15 mers should be possible, but it is not shown here for clarity.